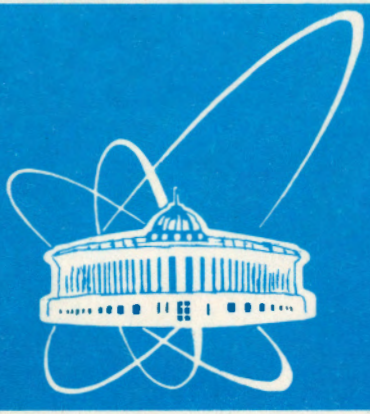

сообщения
объединенного
института
ядерных
исследований
дубна

E14-94-99

F.Prokert*, B.N.Savenko, A.M.Balagurov

THERMAL DIFFUSE SCATTERING IN TIME-OF-FLIGHT NEUTRON DIFFRACTION STUDIED ON SBN SINGLE CRYSTALS

*Research Center Rossendorf, IIM, Germany

1994

Прокерт Ф., Савенко Б.Н., Балагуров А.М. E14-94-99

Исследование теплового диффузного рассеяния в кристаллах SBN с помощью дифракции нейтронов по времени пролета

На нейтронном дифрактометре по времени пролета ДН-2, установленном на импульсном реакторе ИБР-2 в Дубне, исследованы смешанные монокристаллы $SR_xBa_{1-x}Nb_2O_6$ (SBN-x) различного состава ($0.50 < x < 0.75$) в интервале температур от 15 до 773 К. Обнаружено сильное влияние теплового диффузного рассеяния (ТДР) на дифракционную картину. Появление ТДР от длинноволновых вибрационных акустических мод в монокристалле характеризуется отношением скорости звука к скорости нейтрона. Благодаря природе дифракции Лауэ по времени пролета, используемой на дифрактометре ДН-2, ТДР вокруг брэгговских пиков имеет довольно сложный профиль. Понимание природы ТДР вблизи брэгговских пиков имеет большое значение, так как позволяет отделить диффузное рассеяние, появляющееся при диффузном сегнетоэлектрическом фазовом переходе в кристаллах SBN.

Работа выполнена в Лаборатории нейтронной физики ОИЯИ.

Сообщение Объединенного института ядерных исследований. Дубна, 1994

Prokert F., Savenko B.N., Balagurov A.M. E14-94-99

Thermal Diffuse Scattering in Time-of-Flight Neutron Diffraction Studied on SBN Single Crystals

At the time-of-flight (TOF) diffractometer DN-2, installed at the pulsed reactor IBR-2 in Dubna, $Sr_xBa_{1-x}Nb_2O_6$ mixed single crystals (SBN-x) of different compositions ($0.50 < x < 0.75$) were investigated between 15 and 773 K. The diffraction patterns were found to be strongly influenced by the thermal diffuse scattering (TDS). The appearance of the TDS from the long-wavelength acoustic modes of vibration in single crystals is characterized by the ratio of the velocity of sound to the velocity of neutron. Due to the nature of the TOF Laue diffraction technique used on DN-2, the TDS around Bragg peaks has a rather complex profile. An understanding of the TDS close to Bragg peaks is essential in allowing the extraction of the diffuse scattering occurring at the diffuse ferroelectric phase transition in SBN crystals.

The investigation has been performed at the Laboratory of Neutron Physics, JINR.

Communication of the Joint Institute for Nuclear Research. Dubna, 1994

1 Introduction

In connection with the study of single crystals at pulsed neutron sources the questions concerning the separation of the components of diffuse scattering from the Bragg scattering have been subject of increased interest in the last time. In two basic papers [1],[2] the nature of thermal diffuse scattering (TDS) which occurs close to the Bragg reflections in time-of-flight (TOF) neutron diffraction was discussed in detail.

The experimental data obtained on pyrolytic graphite [3], and on single crystals of barium fluoride [4] and calcium fluoride [5] were found to agree with the theoretical predictions. These experiments were performed at the ISIS Pulsed Neutron Facility on the high-resolution powder diffractometer (HRPD) nearly in back scattering ([3] with 2θ=174°) as well as on the single-crystal diffractometer (SXD) using smaller scattering angles ([4] around 2θ=90° and 2θ=125.5°).

In our studies of diffuse phase transition (PT) of mixed single crystal of $Sr_xBa_{1-x}Nb_2O_6$ (SBN-100x) [6], [7] the peak shape of some Bragg reflections indicates that the obtained intensities around the peak position are clearly influenced by phonon scattering. Especially in this case the latter must be

separated from more specific diffuse (quasi-) elastic component which occurs at the diffuse ferroelectric PT. For that reason we intended to study the effects of TDS in SBN explicitly. In the present paper some typical experimental results from different SBN compositions are given in comparison with the theoretical predictions.

2 Theoretical aspects

As shown in [1, 2], the white beam case, dealing with pulsed neutrons scattered at a fixed angle, has unusual features which do not occur in the monochromatic case. The appearance of the TDS from the long-wavelength acoustic modes of vibration in single crystals in the Laue TOF diffraction technique is characterized by the ratio of the velocity of sound c_s to the velocity of the neutron v_n

$$\beta = c_s/v_n. \tag{1}$$

Due to variation of β-ratio with the lattice spacing the TDS around the Bragg peaks may change their profile for different reflections very drastically.

Following [4], in TOF neutron diffraction from a single crystal, TDS from the acoustic modes of vibration occur in the neighbourhood of the Bragg peaks. There are three regions of neutron velocity v_n to be considered in calculating the nature of this scattering.

- If $\beta < 1$

$$v_n > c_s \ , \tag{2}$$

the TDS rises to a maximum at the Bragg peak and scattering is allowed at all points in the reciprocal space (Fig.1a).

- If $\beta > 1 > \beta cos\theta$

$$c_s > v_n > c_s \cos\theta \ , \tag{3}$$

where θ is half the scattering angle, the TDS rises to a steep maximum on either side of the Bragg peak at θ_B, and scattering between these maxima is forbidden (Fig.1b).

- If $\beta cos\theta > 1$

$$c_s \cos\theta > v_n \ , \tag{4}$$

there is *one maximum* only, and this is associated with *phonon creation* for $\theta > \theta_B$ and *phonon annihilation* for $\theta < \theta_B$ (Fig.1c).

The third region, already studied in barium fluoride [4] on SXD at ISIS, is investigated in present paper. The theoretical predictions can been examined now using SBN crystals for which the elastic constants are known rather completely.

In this case the phonon intensity (Eq. 5) (taken from Eq. 26 of [1]) for annihilation (phonon absorption) ($\epsilon = -1$) and creation (phonon emission) ($\epsilon = +1$) is separated.

$$\left(\frac{d\sigma}{d\Omega}\right)^{inel}_{coh,\epsilon} = \frac{k}{k_0}\frac{N}{2}\sum_j \frac{n_j(\mathbf{q})}{\omega_j(\mathbf{q})}|G_j(\mathbf{Q})|^2|J_\epsilon|^{-1}. \tag{5}$$

Here (with the same notation and definitions as used in [1]) $n_j(\mathbf{q})$ are quantum number of phonon modes, given in Eq. 6 and $G_j(\mathbf{Q})$ the *one-phonon scattering structure factor.*

$$n_j(\mathbf{q}) = \{exp[\hbar\omega_j(\mathbf{q})/k'_B T] - 1\}^{-1} \ , \tag{6}$$

where k'_B is Boltzmann's constant and T the absolute temperature. From (5) it follows that the scattering cross section for annihilation and creation differ only by the Jacobian term

$$|J_\epsilon|^{-1} = 1 + (\epsilon\hbar/2E)\,\mathbf{k}\cdot grad_q[\omega_j(\mathbf{q})]. \tag{7}$$

At the observation of acoustic phonon scattering in the diffraction pattern one has to consider the elastic anisotropy of the crystals. The elastic constants of a crystal are represented by a fourth-rank tensor, so that cubic, as well as noncubic, crystals are elastically anisotropic. Only for isotropic sound propagation, the group velocity and phase velocity are the same. As shown in [2] the anisotropy enters into the basic formulae of [1] by replacing $\beta = c_s/v_n$ by β_g containing the group velocity in the characteristic quotient.

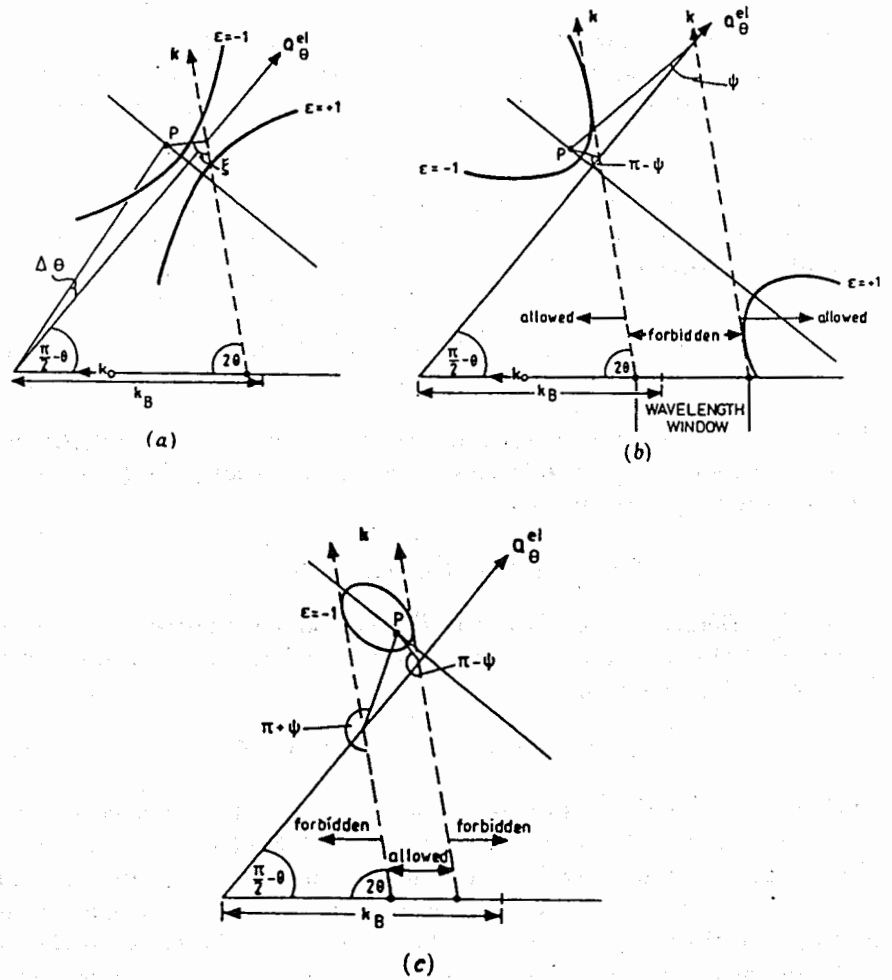

Figure 1: Drawings are taken from [1] to illustrate the change in the one-phonon scattering surface with increasing β.
(a) $\beta < 1$, (b) $\beta > 1 > \beta\cos\theta$, and (c) $\beta\cos\theta > 1$.
The reciprocal-lattice point P is reached in elastic scattering at the Bragg conditions $2\theta = 2\theta_B$, $|\mathbf{k}| = |\mathbf{k}_0| = k_B$. The diagrams are drawn for isotropic sound velocities and for $\theta = 40°$, $\Delta\theta = +6°$. The broken lines are vectors parallel to the scattered beam; TDS takes place when these vectors intersect the scattering surfaces, indicated by heavy lines

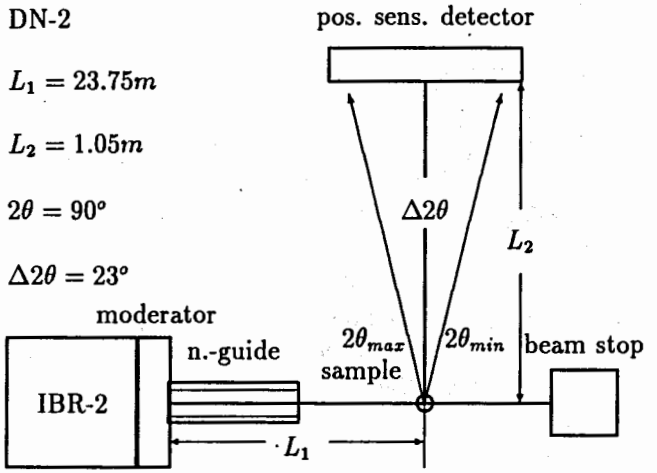

Figure 2: Sketch of the experimental setup used at the TOF diffractometer DN-2.
For $L_2 = 1.05$ m between the 32 detection positions of the full (half) length of the PSD angular steps $\Delta 2\theta$ of 46' (23') are given . The full detector array covers a $\Delta 2\theta$-range of $\pm 11.9°$

3 TOF study of TDS from $Sr_xBa_{1-x}Nb_2O_6$

3.1 TOF spectrometer setup

The experiments were done on the single crystal TOF spectrometer DN-2 (Fig.2) installed at the pulsed reactor IBR-2 of the JINR in Dubna [8].

The instrument has a long primary flight path L_1 (partly within a neutron guide). Using a one-dimensional position sensitive detector (PSD) diffraction patterns are taken from a sectorial area of the reciprocal space around the chosen direction (Fig.3). In consequence of the short distance from sample to PSD the secondary flight path $L_2 \ll L_1$. In the here discussed experiments the scattering angle for the detector central position 2θ was fixed at 90°.

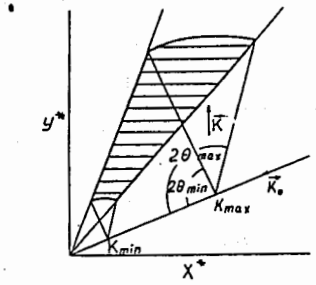

Figure 3: Observed region of the reciprocal space (x^*, y^* coordinates) determined by the interval of the experimental coordinates k and 2θ : $k_{min} \leq k \leq k_{max}$ and $2\theta_{min} \leq 2\theta \leq 2\theta_{max}$

SBN-100x mixed single crystals of different compositions (0.50≤x≤0.75) were investigated between 15 K and 773 K in a refrigerator cryostat and a furnace, respectively.

3.2 The elastic properties of SBN single crystals

At room temperature (RT) $Sr_xBa_{1-x}Nb_2O_6$ mixed single crystals are (pseudo-) tetragonal in the composition range $0.75 \geq x \geq 0.25$. (Tungsten bronze structure with lattice parameters $a \sim 12.43$ Å and $c \sim 3.91$ Å at RT.) In analogy to the Cauchy relation for the elastic stiffness constants of cubic crystals

$$c_{11} - c_{12} - 2c_{44} = 0 \,, \tag{8}$$

such a tetragonal crystal is elastically isotropic if the relation

$$g \equiv c_{11} - c_{12} - 2c_{66} = 0 \tag{9}$$

is fulfilled.

The relevant stiffness constants are known. They have been determined by piezoelectric resonance methods [10], [9] and by phonon dispersion measurements by means of inelastic neutron scattering [11]. Despite the fact that there are considerable differences between the two sets of the elastic constants (see Table 1), the isotropy relation is nearly fulfilled for both.

Table 1: Comparison of elastic stiffness constants of SBN measured piezoelectrically (p) and by neutrons (n)

$c_{11}/10^{10}Nm^{-2}$	$c_{12}/10^{10}Nm^{-2}$	$c_{66}/10^{10}Nm^{-2}$	g	Ref.	Method
24.1	13.4	5.2	0.3	[11]	n
18.8	7.4	5.2 from [11]	1.0	[10],[9]	p

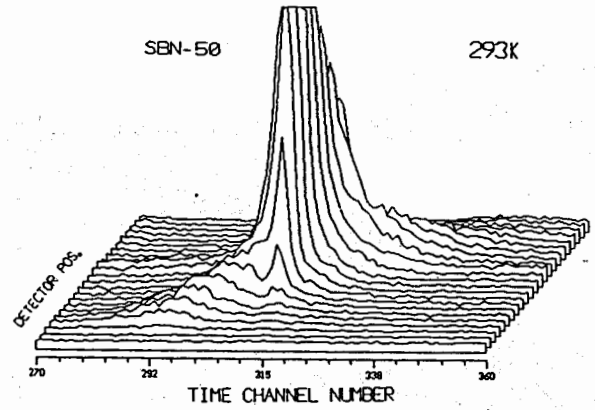

Figure 4: 3d-plot of (002) reflection of SBN-50 around $2\theta = 92.4°$. (2θ-range $86.3° - 98.5°$, ch_w =64 μs)

3.3 Results of β-parameter fitting

Especially some of the strong *(00l) reflections of SBN* recorded at the scattering plane (110) and (100), respectively, were found to be *strongly influenced by thermal diffuse scattering (TDS)* (Fig. 4). Fig.4 gives a picture of the 'TDS-wings' around the strong (002) peak of SBN-50 in a 3d-plot.

Fig.5 shows the TDS at a contour plot of intensity recorded at room temperature (RT) for $2\theta = 90°$ from a SBN-50 sample around the (002) reciprocal lattice point. For a given $\Delta 2\theta$ the TDS occurs only on one side of the Bragg peak (t_B, $2\theta_B$). As expected from the theory for the case $\beta cos\theta > 1$ the TDS appears at shorter times-of-flight than t_B if $2\theta < 2\theta_B$ and at longer times if $2\theta > 2\theta_B$.

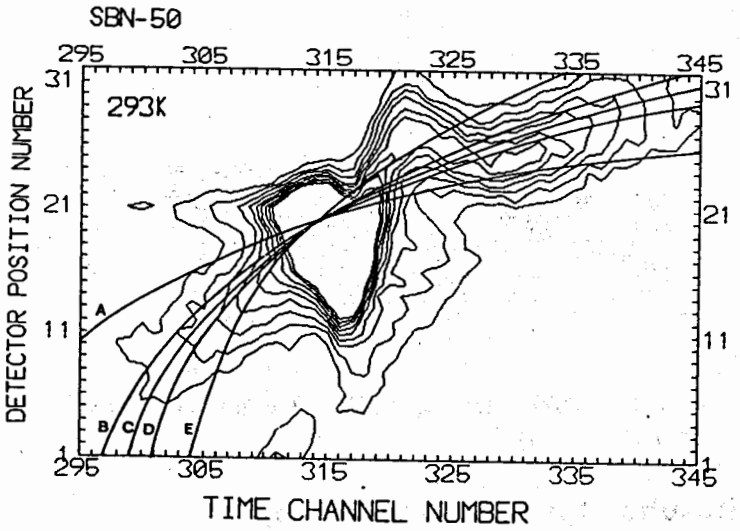

Figure 5: Contour plot of (002) reflection of SBN-50 around $2\theta = 92.4°$. The detector positions $1 - 32$ cover the 2θ-range $86.3° - 98.5°$. Time channel width ch_w =64 μs. The curves A, B, C, D, and E are calculated for c_s= 2.5, 2.8, **2.9**, 3.0, and 3.3 kms^{-1} giving the parameter values β: 1.77, 1.98, **2.05**, 2.13, and 2.35. The crossing of these curves marks the position of the Bragg peak: t_B, $2\theta_B$

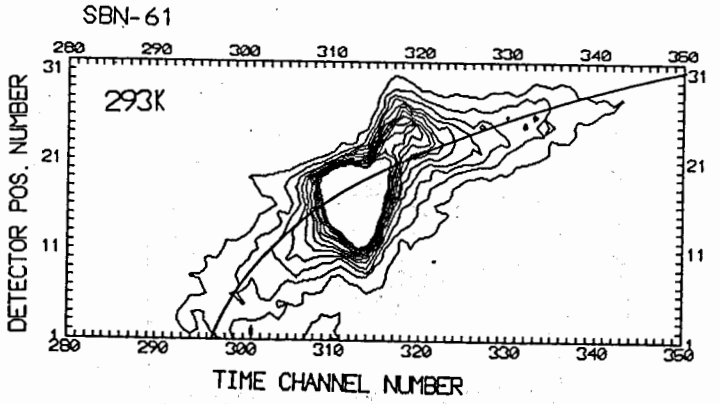

Figure 6: Plot of (002) reflection of SBN-61 around $2\theta = 90°$. (2θ-range $83.9° - 96.1°$; $ch_w = 64\ \mu s$)

By a variation of the β-parameter different curves were calculated for the central position of the TDS, using the relation of Eq. 12 from [5]

$$\Delta t/\Delta 2\theta = \frac{1}{2} t_B(\tan\theta)/(\beta^2 \cos^2\theta - 1). \qquad (10)$$

From the curve fitting (with curve C) a phonon velocity of $c_s = 2.90\ kms^{-1}$ was approximated. This value also fits the TDS pattern measured at RT on a SBN-61 single crystal around (002) (Fig.6).

This fitted value of the phonon phase velocity is not far from the value $c_s^{calc} = 3.16\ kms^{-1}$ determined directly for the elastically isotropic case from the elastic constant $c_{44} = (5.2 \pm 0.5)\ 10^{10} Nm^{-2}$ and the density $\rho = 5.2\ gcm^{-3}$.

Around the (001) Bragg reflection in SBN the contributions of phonon scattering were found to be quite small. In the pattern (Fig.7) the TDS at RT is covered by other kinds of diffuse scattering.

The dependence of the TDS on temperatures higher than room temperature (RT) is demonstrated in Fig.8. Fig.9 shows the reducing of the TDS at low temperature (20 K) beside a clear change of intensity contour shape , which could be caused by structural transitions. The variation of

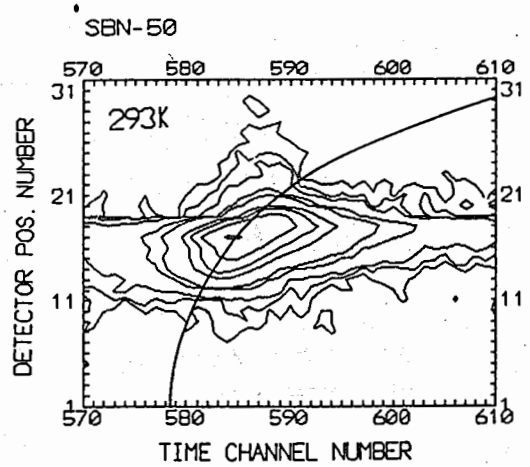

Figure 7: Plot of (001) reflection of SBN-50 around $2\theta = 90°$. Diffuse scattering mainly due to other processes than TDS. (2θ-range $78.5° - 101.5°$; ch_w =64 μs)

intensity comes from the temperature dependence of quantum number of the phonon modes $n_j(q)$ (Eq. 6). For $q \approx 10^{-2} \cdot Q_B^{(002)}$ follows a phonon energy $\hbar\omega_j(\mathbf{q}) \approx 0.5\ meV$ and we get $n_j^{20} \approx 3$, $n_j^{293} \approx 60$, and $n_j^{700} \approx 120$. Comparing the intensities for phonon annihilation and phonon creation in SBN around (002) one sees higher values for annihilation in accordance with the theory (Eq. 7) .

As shown in [1] for elastically isotropic material the Jacobian becomes

$$J_\epsilon = 1 + \epsilon\beta \tag{11}$$

and gives the relation

$$\frac{\left(\frac{d\sigma}{d\Omega}\right)^{annihl}_{\epsilon=-1}}{\left(\frac{d\sigma}{d\Omega}\right)^{creat}_{\epsilon=+1}} = \frac{|J_{-1}|^{-1}}{|J_{+1}|^{-1}} = \frac{|1-\beta|^{-1}}{|1+\beta|^{-1}} = \frac{|1+\beta|}{|1-\beta|}. \tag{12}$$

With $\beta_{(002)}^{SBN} \approx 2$ we get a ratio of $\approx$3.

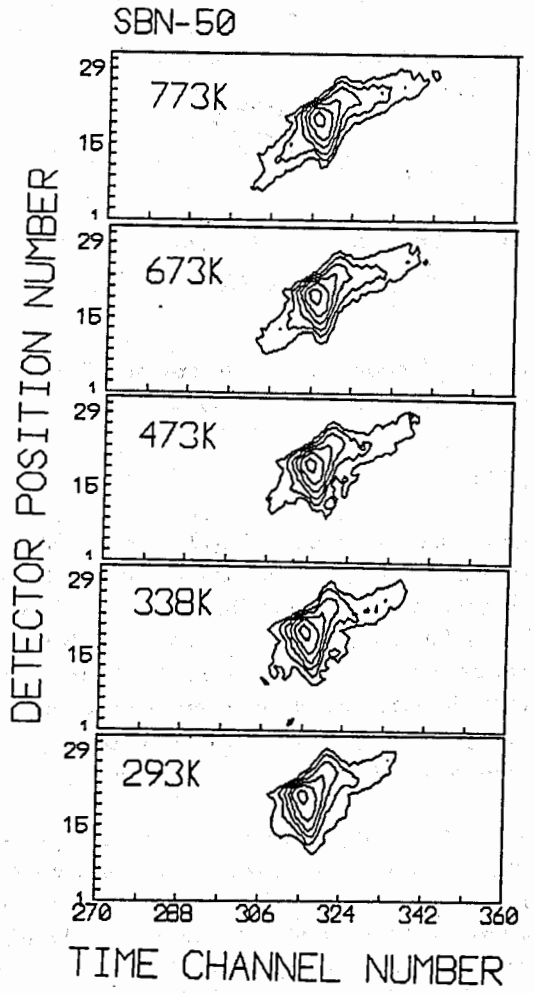

Figure 8: Plot of (002) reflections of SBN-50 around $2\theta = 90°$ at RT and above (773, 673, 473, and 338 K). (2θ-range $78.5° - 101.5°$; ch_w =64 μs)

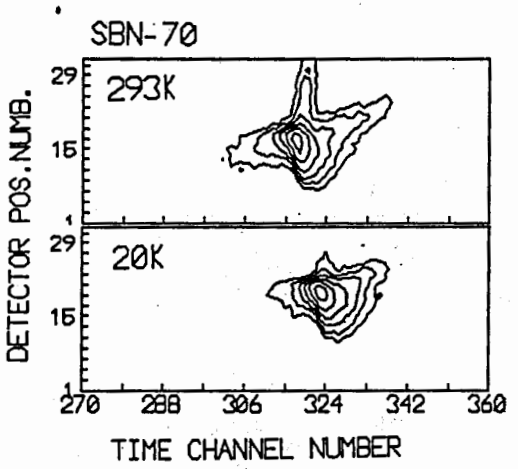

Figure 9: Plot of (002) reflections of SBN-70 around $2\theta = 90°$ at RT and below (20 K). (2θ-range $78.5° - 101.5°$; ch_w =64 μs)

4 Discussion

The given results show that in $Sr_xBa_{1-x}Nb_2O_6$ single crystals at the here selected scans around the Bragg reflections the features of the diffuse scattering pattern are dominated by the contributions of the long-wave length acoustic phonons. This follows from the characteristic distribution of the TDS which shows an excellent accordance with the theory. Further it follows qualitatively from the occurrence of the theoretically expected changes of TDS intensity with temperature and from the proof of the expected intensity differences between emission and absorption of phonons.

Supposing SBN to be nearly elastically isotropic, the measured phonon velocity may be compared directly with the phase velocity c_s^{calc} calculated form elastic stiffness constant c_{44}. The existing small difference of - 8 % does not exceed the error level of the constant c_{44}. However, the here used method is more accurate (see,e.g., [1]) than the normaly used extrapolation of the measured slope of the phonon branch to small q-values.

For the analysis of the shape of the diffuse scattering at temperatures higher as well as at lower than RT one should take into account that phonon contribution itself and the other parts of diffuse scattering resulting from structrual disorder may be changed by the occurrence of structural phase transitions of different types ([6],[7]). For these reasons only rough estimations were used for interpretation.

Acknowledgement

This work has been supported in part by the BMFT under registration sign 03-GO3ROS-5.

References

[1] B.T.M. Willis
Acta Cryst. **A42**, 514 (1986)

[2] P. Schofield and B.T.M. Willis
Acta Cryst. **A43**, 803 (1987)

[3] B.T.M. Willis, C.J. Carlile, R.C. Ward, W.I.F. David, and M.W. Johnson
Europhys. Lett. **2**, 767 (1986)

[4] C.J. Carlile, D.A. Keen, C.C. Wilson, and B.T.M. Willis
Acta Cryst. **A48**, 826 (1992); ISIS Exp.Report 1991, A78

[5] C.J. Carlile and B.T.M. Willis
Acta Cryst. **A45**, 708 (1989)

[6] A.M. Balagurov, F. Prokert, and B.N. Savenko
phys. stat. sol. (a) **103**, 131 (1987)

[7] F. Prokert, A.M. Balagurov, D. Sangaa, and B.N. Savenko
Ferroelectrics **124**, 124 (1991)

[8] I.M. Frank and P. Pacher
Physica **B120**, 37 (1983)

[9] S. T. Liu
Ferroelectrics **22**, 709 (1978)

[10] S. T. Liu and L. E. Cross
phys. stat. sol. (a) **41**, K83 (1977)

[11] F. Prokert
phys. stat. sol. (b) **113**, 239 (1982)

Received by Publishing Department
on March 24, 1994.